








Impact of the gradient in gantry-table rotation on dynamic trajectory radiotherapy plan quality

Hannes A. Loebner¹  | Silvan Mueller¹  | Werner Volken¹ |
 Philipp Wallimann¹  | Daniel M. Aebersold¹  | Marco F. M. Stampanoni²  |
 Michael K. Fix¹  | Peter Manser¹ 

¹Division of Medical Radiation Physics and Department of Radiation Oncology, Inselspital, Bern University Hospital and University of Bern, Bern, Switzerland

²Institute for Biomedical Engineering, ETH Zürich and PSI, Villigen, Switzerland

Correspondence

Hannes A. Loebner, Abteilung fuer medizinische Strahlenphysik, Friedbuehlschulhaus, Freiburgstrasse 18, 3010 Bern, Switzerland.
 Email: Hannes.Loebner@insel.ch

Funding information

Varian

Abstract

Background: To improve organ at risk (OAR) sparing, dynamic trajectory radiotherapy (DTRT) extends VMAT by dynamic table and collimator rotation during beam-on. However, comprehensive investigations regarding the impact of the gantry-table (GT) rotation gradient on the DTRT plan quality have not been conducted.

Purpose: To investigate the impact of a user-defined GT rotation gradient on plan quality of DTRT plans in terms of dosimetric plan quality, dosimetric robustness, deliverability, and delivery time.

Methods: The dynamic trajectories of DTRT are described by GT and gantry-collimator paths. The GT path is determined by minimizing the overlap of OARs with planning target volume (PTV). This approach is extended to consider a GT rotation gradient by means of a maximum gradient of the path (G_{max}) between two adjacent control points ($G = |\Delta\text{table angle}/\Delta\text{gantry angle}|$) and maximum absolute change of G (ΔG_{max}). Four DTRT plans are created with different maximum G and ΔG : G_{max} and $\Delta G_{max} = 0.5$ and 0.125 (DTRT-1), 1 and 0.125 (DTRT-2), 3 and 0.125 (DTRT-3) and 3 and 1 (DTRT-4), including 3–4 dynamic trajectories, for three clinically motivated cases in the head and neck and brain region (A, B, and C). A reference VMAT plan for each case is created. For all plans, plan quality is assessed and compared. Dosimetric plan quality is evaluated by target coverage, conformity, and OAR sparing. Dosimetric robustness is evaluated against systematic and random patient-setup uncertainties between ± 3 mm in the lateral, longitudinal, and vertical directions, and machine uncertainties between $\pm 4^\circ$ in the dynamically rotating machine components (gantry, table, collimator rotation). Delivery time is recorded. Deliverability and delivery accuracy on a TrueBeam are assessed by logfile analysis for all plans and additionally verified by film measurements for one case. All dose calculations are Monte Carlo based.

Results: The extension of the DTRT planning process with user-defined G_{max} and ΔG_{max} to investigate the impact of the GT rotation gradient on plan quality is successfully demonstrated. With increasing G_{max} and ΔG_{max} , slight (case C, $D_{mean, parotid\ l.}$: up to -1 Gy) and substantial (case A, $D_{0.03cm^3, optic\ nerve\ r.}$: up to -9.3 Gy, case B, $D_{mean, brain}$: up to -4.7 Gy) improvements in OAR sparing are observed compared to VMAT, while maintaining similar target coverage. All plans are delivered on the TrueBeam. Expected and actual machine position values recorded in the logfiles deviated by $<0.2^\circ$ for gantry, table and collimator rotation. The film measurements agreed by $>96\%$ (2% global/2 mm Gamma

This is an open access article under the terms of the [Creative Commons Attribution-NonCommercial-NoDerivs](https://creativecommons.org/licenses/by-nc-nd/4.0/) License, which permits use and distribution in any medium, provided the original work is properly cited, the use is non-commercial and no modifications or adaptations are made.

© 2023 The Authors. *Medical Physics* published by Wiley Periodicals LLC on behalf of American Association of Physicists in Medicine.

passing rate) with the dose calculation. With increasing G_{max} & ΔG_{max} , delivery time is prolonged by <2 min/trajectory (DTRT-4) compared to VMAT and DTRT-1. The DTRT plans for case A and B and the VMAT plan for case C plan reveal the best dosimetric robustness for the considered uncertainties.

Conclusion: The impact of the GT rotation gradient on DTRT plan quality is comprehensively investigated for three cases in the head and neck and brain region. Increasing freedom in this gradient improves dosimetric plan quality at the cost of increased delivery time for the investigated cases. No clear dependency of GT rotation gradient on dosimetric robustness is observed.

KEYWORDS

dynamic trajectory radiotherapy, non-coplanar radiotherapy, treatment plan quality

1 | INTRODUCTION

To improve organ at risk (OAR) sparing and target coverage, research in intensity modulated radiotherapy on C-arm linear accelerators (linacs) has explored the possibility to increase the degrees of freedom (DoF) during treatment planning and delivery compared to three-dimensional conformal radiotherapy. C-arm linacs have the possibility to dynamically move multiple machine axes simultaneously: volumetric modulated arc therapy (VMAT) combines multi-leaf collimation (by means of the photon multi-leaf collimator, MLC) and dynamic gantry rotation to efficiently deliver intensity modulated photon beams. VMAT has become standard of care in radiotherapy.^{1–3} For a typical VMAT plan, the beam directions reside within a two-dimensional plane. Previous studies confirm however, that by deviating from this plane, improvements in dosimetric plan quality, particularly in OAR sparing, are achievable.^{4–8} Consequently, several treatment techniques employing non-coplanar beam directions have been developed, such as non-coplanar partial VMAT arcs (e.g., Hyper Arc^{9,10}) or 4π -IMRT.^{11–14} Moreover, dedicated systems such as the CyberKnife[®] (Accuray, Sunnyvale, CA, USA) or the discontinued VERO[®] (Brainlab, Munich, Germany and Mitsubishi Heavy Industries, Tokyo, Japan) are explicitly developed to use non-coplanar beam angles. However, these systems are not as widely available as C-arm linacs.

On the downside, non-coplanar treatment techniques present a challenge in preventing collisions between gantry and table, as well as between gantry and patient. Furthermore, diverging from the coplanar plane is usually connected with increased delivery times, especially for 4π -IMRT,^{11,15,16} which can negatively impact patient comfort. Hence, more efficient delivery is desired and can be achieved by combining dynamic gantry and table rotation with intensity modulation^{17,18}: Dynamic trajectory radiotherapy (DTRT)^{19,20} is an extension of VMAT that involves dynamic table and collimator rotations during delivery, allowing for treatment times similar to VMAT.

A comprehensive assessment of the plan quality of DTRT compared to VMAT requires the characterization of the dynamics of DTRT, particularly the gantry-table (GT) rotations, and the evaluation of the following aspects of plan quality²¹:

- *Dosimetric plan quality*
- *Plan complexity*
- *Dosimetric robustness*
- *Deliverability*
- *Delivery time*

Dosimetric treatment plan comparisons considering different treatment sites already indicated substantially improved sparing of OARs for DTRT as compared to VMAT.^{18,19} With the added DoF and the associated increased complexity, the dosimetric robustness of DTRT plans could be compromised. The number of robustness studies including DTRT are limited, and usually focus on patient setup uncertainties.^{22,23} Uncertainties in the now dynamically rotating machine components have not been evaluated. A comprehensive robustness assessment needs to additionally investigate how uncertainties in gantry, table, and collimator, impact the dosimetric plan quality. To ensure deliverability, the treatment machine must meet additional requirements compared to VMAT. Namely, the accurate dynamic rotation of the treatment table and the collimator in combination with the gantry rotation and MLC modulation needs to be verified. On the patient side, the delivery time can impact patient comfort. Delivery time is therefore another key quantity to assess when determining plan quality.

Finally, as DTRT trajectories are patient-specific and not limited to a specific GT path, it is crucial to consider and characterize their dynamics when evaluating and comparing the plan quality. For this purpose, we extended the inhouse developed DTRT planning process¹⁹ to consider a user-specified GT rotation gradient. In this work, the extended DTRT planning process is applied to generate DTRT plans with different GT rotation gradients for three clinically motivated cases:

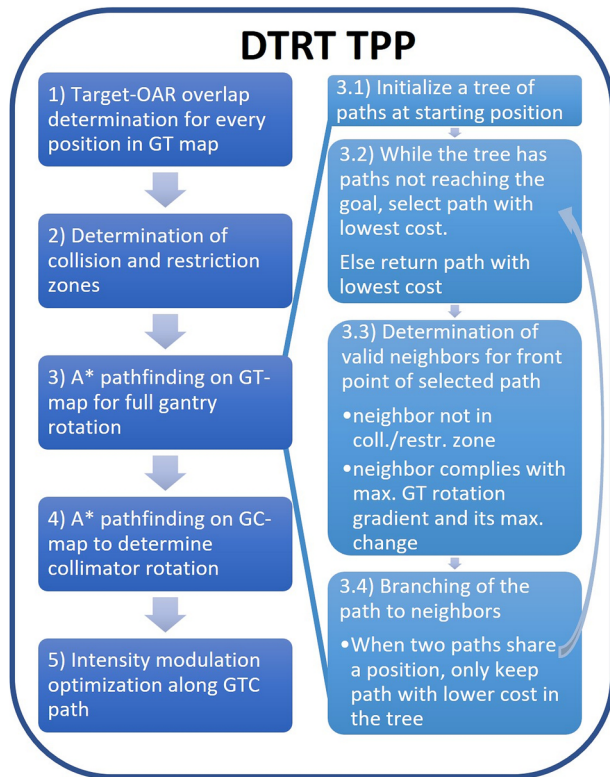


FIGURE 1 Steps of the DTRT TPP, with the path finding in detail shown on the right.

two head and neck cases and one brain case. The VMAT and DTRT plans were used to study the trade-offs between dosimetric plan quality, plan complexity, dosimetric robustness, deliverability and delivery time as a function of the GT rotation gradient.

2 | MATERIALS AND METHODS

A GT rotation gradient is introduced to characterize the dynamics of DTRT trajectories. The GT rotation gradient is defined as the ratio of the change in table angle to the change in gantry angle between two adjacent control points of the DTRT trajectory.

2.1 | DTRT treatment planning process

To investigate the impact of the GT rotation gradient on plan quality, the underlying idea for the DTRT treatment planning process (TPP), described by Fix et al.,¹⁹ is extended. In the following the TPP is summarized, and the extended path finding is described in more detail (Figure 1).

The DTRT TPP is started by creation of the target-OAR overlap maps, based on the structure set (Figure 1,1). The target-OAR overlap in the beam's-eye-view is determined geometrically for a set of 400

uniformly²⁴ distributed beam directions defined by a gantry and table angle using an in-house software. First, the 2D overlap of the projection is calculated. Second, the corresponding fractional volume of target and OAR is determined using the mesh of the structures and raytracing. The fractional volumes are weighted according to their depth within the patient body ($weight = e^{-depth/22}$), which corresponds to an approximation of the depth dose curve of a 6 MV photon beam in water, neglecting build-up. Third the weighted fractional volume overlap is determined. OARs located in front of the target are therefore penalized more than those located behind. The weighted overlaps are then projected on a two-dimensional GT map of gantry (x -axis) and table angles (y -axis), ranging from -180° to 180° and -90° to 90° , respectively. Summed maps can be generated for multiple user-selected OARs to emphasize the sparing of OAR groups (target-OARs overlap). The GT map is interpolated to a resolution of $r_g = 2^\circ$ in gantry and $r_t = 0.25^\circ$ in table angle. Beam directions in collision zones (between gantry-patient or GT), as well as CT restriction zones (beam entering through the end of the CT), are excluded in the GT maps (Figure 1,2). An A* algorithm²⁵ is employed to find the GT path for a full gantry rotation in this map, which minimizes the target-OARs overlap (Figure 1,3). The A* algorithm is deterministic and provides the path with the lowest cost on a given cost map. The GT pathfinding can be repeated on different target-OAR overlap maps to obtain multiple paths. In a next step, the dynamic collimator rotation is determined (Figure 1,4). To this end, a gantry-collimator (GC) map is generated for the previously determined GT path using an inhouse software: The GC map quantifies the width in the leaf travel direction of a target-conformal and jaw-defined field for each position along the GT path and all possible collimator rotations. On the GC map, an A* algorithm determines the dynamic collimator rotation along the GT path with minimal summed field width. This dynamic collimator rotation reduces potential leaf travel in the later intensity modulation optimization.

The resulting gantry-table-collimator (GTC) paths are transferred back into a research version of Eclipse® embedded in the Aria 15.6 framework (Varian Medical Systems, Palo Alto, CA, USA) via the Eclipse Scripting Application Programming Interface (ESAPI). In Eclipse, the GTC paths are then defined by the standard control point resolution for a full VMAT arc (178 control points). A research version of the Eclipse photon optimizer is used to optimize the intensity modulation and generate the treatment plan according to dosimetric clinical guidelines (Figure 1,5).

The dose calculations in this work are Monte Carlo (MC) based using the Swiss Monte Carlo Plan (SMCP).²⁶ SMCP employs VMC++²⁷ for the radiation transport through the beam modifiers and the dose distribution calculation within the patient. Calculation voxel

size is $0.25 * 0.25 * 0.25 \text{ cm}^3$. The number of simulated primary particles per calculation is in the order of 10^8 , leading to an actual mean statistical uncertainty of $<1.2\%$ (one standard deviation) for the voxels with dose values higher than 50% of the maximum dose for all presented dose distributions.

To steer the path finding of the GT path, step 3 of the DTRT TPP is expanded to consider user-defined limitations given by a maximal GT rotation gradient G_{max} and its change ΔG_{max} between two adjacent positions of the GT path along the gantry axis (pseudo code in Supplementary Material 0). G_{max} restricts the steepness of the resulting path. The motivation to introduce G_{max} is to control the maximal slow-down of the gantry rotation speed due to the table rotation. Introducing G_{max} gives the possibility of aiming for similar delivery times as VMAT. ΔG_{max} limits the maximal directional change and enables granular adjustment of the smoothness of the resulting path. Limiting unsmooth behavior in the table rotation can increase machine durability and can reduce unwanted patient motion during delivery.

GT path finding is performed in a three-dimensional map, where the third dimension is used to consider the change in table angle and thus to enable finding the optimal path under the additional restriction of ΔG_{max} . A position in this map is given by $p_{i,j,k}$:

- $i \in [1, I = 360^\circ/r_g + 1]$ corresponds to the gantry angle $g_i = -180^\circ + (i - 1) * r_g$.
- $j \in [1, J = 180^\circ/r_t + 1]$ corresponds to the table angle $t_j = -90^\circ + (j - 1) * r_t$.
- $k \in [1, K = 2G_{max} * r_g/r_t + 1]$ is an index whose value range defines the permissible table positions. The change in table angle $\Delta t_k = (-G_{max} * r_g + (k - 1) * r_t)$ (Equation 1) between two adjacent positions along the GT path is dependent on k .

Owing to the third dimension, the potential neighbors of each position can be determined independently of the pathfinding while respecting the constraints of G_{max} and ΔG_{max} . Each $p_{i,j,k}$ has an associated cost $c_{i,j}$ (independent of k , which refers to permissible table position at gantry-table position indexed by i and j). The cost corresponds to the target-OARs overlap for the respective beam direction and is independent of index k , and thus the notation of this cost can be reduced to $c_{i,j} = c_{i,j,k}$.

γ^a is the GT path with index a for a full gantry rotation and consists of I positions with the assigned labels $(j_1^a, j_2^a, \dots, j_I^a)$, which can be translated to the respective table angle for each $i = 1, \dots, I$. For a path, $\Delta t_{k_i^a}$ can directly be calculated by $\Delta t_{k_i^a} = t_{j_{i-1}^a} - t_{j_i^a}$ and index k_i^a can be obtained by solving Equation (1) for k . A path γ^a needs to comply with the following restrictions for all i :

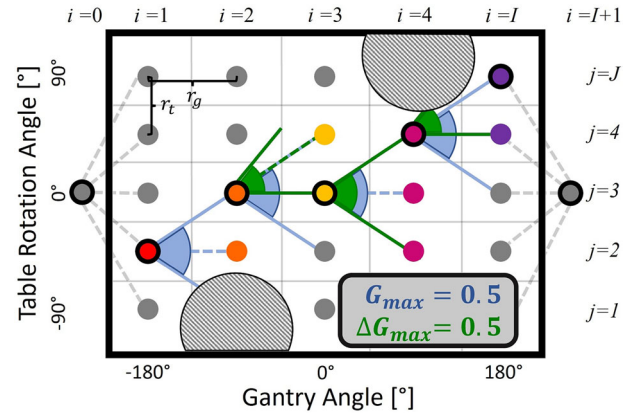


FIGURE 2 Schematic representation to determine the neighbors of specific positions within the GT map. The resolution in table and gantry angle is adapted for demonstration purpose. To the left and right side of the map, artificial start and end positions are shown. The black encircled points have neighboring candidates that are exemplary shown in different colors: the neighbors of the red points are displayed in orange, the orange points' neighbors are displayed in yellow, the yellow points' neighbors are displayed in magenta, and the purple points neighbor the magenta points. The blue and green cones represent the G_{max} and ΔG_{max} restriction, respectively. The dashed half-circles indicate collision and CT-restriction zones. Per definition, the ΔG_{max} restriction is only applicable starting from $i = 2$.

- All p_{i,j_i^a,k_i^a} of path γ^a cannot be in a collision or restriction zone
- $G_i = \left| \frac{t_{j_i^a} - t_{j_{i+1}^a}}{g_i - g_{i+1}} \right| \leq G_{max}$
- $\Delta G_i = \left| \frac{t_{j_{i-1}^a} - t_{j_i^a}}{g_{i-1} - g_i} - \frac{t_{j_i^a} - t_{j_{i+1}^a}}{g_i - g_{i+1}} \right| = \left| \frac{\Delta t_{k_i^a}}{g_{i-1} - g_i} - \frac{\Delta t_{k_{i+1}^a}}{g_i - g_{i+1}} \right| \leq \Delta G_{max}$

Additionally, an artificial start p_0 and end position p_{I+1} with no cost ($c_0 = c_{I+1} = 0$) are introduced. Gantry and table angle and k are not defined for p_0 and p_{I+1} . All p_{1,j_1,k_1} neighbor p_0 and p_{I+1} neighbors all p_{i,j_i,k_i} . Introducing an artificial start and end position enables finding the path with the optimal start and end position on the map, without introducing a bias by an arbitrary selection of the start and end table angle (Figure 2).

The path cost between two positions is given by the mean of the position costs. The goal is to find the GT path γ^* which has the minimal path cost C_{γ^*} out of all paths A which comply with the above criteria. The optimization problem reads as follows:

find γ^* , such that

$$C_{\gamma^*} = \min_{\gamma^a \in A} \left(\sum_{i=0}^I \frac{1}{2} * (c_{i,j_i^a} + c_{i+1,j_{i+1}^a}) \right)$$

The A* algorithm starts at p_0 . From there, it establishes and iteratively expands a tree of paths to find the path

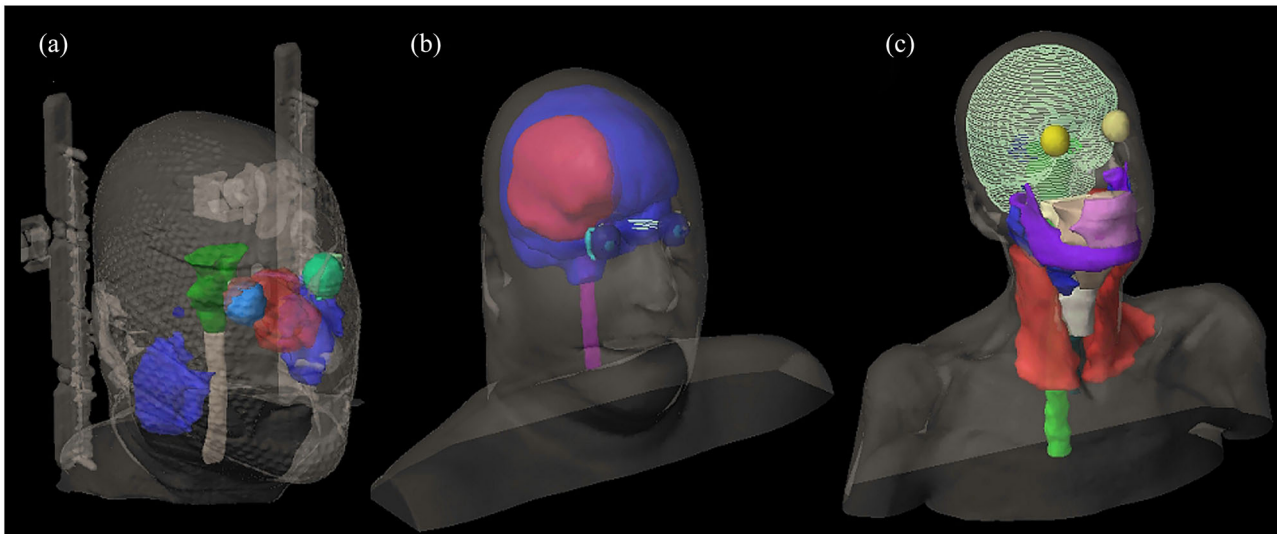


FIGURE 3 The investigated nasopharynx (A), glioblastoma (B) and bilateral oropharynx case (C) are shown. The PTV is shown in red, the OARs are visualized in different colors.

TABLE 1 G_{max} and ΔG_{max} specifications for the considered VMAT and DTRT plans.

	VMAT	DTRT-1	DTRT-2	DTRT-3	DTRT-4
G_{max}	0	0.5	1	3	3
ΔG_{max}	0	0.125	0.125	0.125	1

with the lowest cost for a full gantry rotation. A priority queue is used to expand only the paths with the current lowest path cost. The extended path finding considers the above-mentioned restrictions at the stage of neighbor determination $p_{i+1\#}, j_{i+1\#}, k_{i+1\#}$ of p_{i,j_i^a, k_i^a} prior to the path finding.

An essential feature of the A* algorithm to substantially improve efficiency is the bookkeeping which enables discarding paths from the tree of paths when two paths share a position (equal in all three coordinates). Only the path corresponding to the lower path cost is kept. The suspension of paths of higher cost substantially reduces the number of paths that are expanded during the path finding.

2.2 | Clinically motivated cases

Three representative cases in the head and neck and brain region are investigated: a nasopharynx case (A), a glioblastoma case (B), and a bilateral oropharynx case (C) (Figure 3). For each case, a coplanar VMAT plan is created as a reference plan. To investigate the impact of the GT rotation gradient, four DTRT plans conforming to different G_{max} & ΔG_{max} are created for each case (Table 1).

A suitable set of optimization objectives is determined for each case to optimize the VMAT and DTRT plans

alike, aiming for similar target coverage between the plans (Supplementary Material 1). VMAT and DTRT plans are optimized using the same optimizer (i.e., a research version of the Eclipse photon optimizer, which allows for additional dynamic machine components, table and collimator rotation, during the optimization).

In Table 2, the prescription, VMAT arc setup and DTRT strategy are described for case A, B and C. The different dynamic trajectories focus on the sparing of different OAR groups by considering the overlap of the target with different OARs. In cases, where the field width of the arc/dynamic trajectory in the leaf travel direction would exceed 10 cm, field splitting is performed to enable more MLC leaf modulation. Field splitting is always performed in leaf-travel direction by dividing the field-of-view with an overlap of 2 cm in the center to generate two arcs/dynamic trajectories. For cases A, B, and C, the CTV-PTV expansion is 0.3 cm, 0.5 cm, and 0.5 cm, respectively. When a distance between PTV to skin surface of 0.5 cm could not be maintained, the CTV-PTV expansion is reduced accordingly.

2.3 | Evaluation

2.3.1 | Plan complexity

Plan complexity is evaluated using the average G and ΔG of the final paths, as well as the modulation complexity score (MCS). The MCS was originally introduced for IMRT,²⁸ and then extended to VMAT.²⁹ In this work, the concept is applied to DTRT plans by transferring the definition of MCS along the control points of the VMAT arc to the control points along the DTRT trajectory. The MCS ranges from 0 to 1, with a higher score indicating a “less complex” plan.

TABLE 2 Prescription and VMAT and DTRT strategy for case A, B, and C.

Treatment site	Prescription	VMAT strategy	DTRT strategy
Case A, nasopharynx	50 Gy to 95% of the PTV, delivered in 25 fractions	Three arcs, with rotated collimator (45° and 90°) for the second and third arc with respect to the first arc	Three dynamic trajectories, <i>first</i> : all OARs, <i>second</i> : optic nerve, <i>third</i> : chiasm—second and third focus on sparing of small important structures
Case B, glioblastoma	60 Gy to 50% of the PTV, delivered in 30 fractions	Two arcs, with the second one duplicated by means of field splitting, with rotated collimator for the first arc (90°) with respect to the second arc	Two dynamic trajectories, with the first one being duplicated by 90° collimator rotation, <i>first</i> : brain—sparing healthy brain tissue, <i>second</i> : right optic nerve—due to its proximity to the target
Case C, bilateral oropharynx	50 Gy to 95% of the PTV, delivered in 25 fractions	Two arcs, duplicated using field splitting, with rotated collimator (90°) with respect to each other	Two dynamic trajectories, which are duplicated by field splitting, <i>first</i> : brain, brainstem, parotids, and oral cavity—OARs in the upper head region, <i>second</i> : pharynx, spinal cord—OARs close to the PTV

2.3.2 | Dosimetric plan quality

Dosimetric plan quality is assessed by three aspects:

- Evaluating target coverage, conformity and OAR sparing in terms of DVH comparison.
- Comparing the Paddick Index³⁰ for the prescription isodose (PI) and for 50% of the prescription ($PI_{50\%}$). The PI is given by: $PI = TV_{PIV}^2 / TV * PIV$, with TV as target volume, PIV as prescription isodose volume and TV_{PIV} as target volume covered by prescription isodose.
- Assessing the low dose bath in the normal tissue ($NT = Body - PTV$) by evaluating $V_{5 Gy,NT}$, and $V_{10 Gy,NT}$ for the respective plans.⁸

Additionally, a comparison of the objective function values of the dose distributions after optimization and final dose calculation for each case can be found in the Supplementary Material 2.

2.3.3 | Dosimetric robustness

A previously developed robustness tool³¹ is used to assess the impact of patient- and machine-related uncertainties on the dose distributions of the plans. On the patient side, systematic patient-setup uncertainties (−0.3 cm, 0.0 cm, 0.3 cm), the combination thereof, and random patient setup uncertainties sampled from a Gaussian distribution ($\sigma = 0.0$ cm and 0.3 cm) and the combination thereof in longitudinal, lateral and vertical direction, are investigated. This leads to a total of $3 \times 3 \times 3 - 1$ (nominal scenario) = 26 systematic and $2 \times 2 \times 2 - 1 = 7$ random patient-setup uncertainty scenarios per plan. On the machine side, systematic uncer-

tainties (−4°, −2°, −1°, 0°, 1°, 2°, 4°) in gantry, table and collimator rotation and the combination thereof are investigated, leading to a total of $7 \times 7 \times 7 - 1 = 342$ machine-related uncertainty scenarios per plan.

Patient-setup uncertainties are selected to include extreme cases observed in clinical practice.³² Furthermore, setup shifts up to 0.3 cm are often not corrected for in clinical practice.³³ Machine uncertainties are selected to evaluate miscalibration scenarios: systematic miscalibrations of the machine components are not visible in the machine logfiles. For DTRT, investigations of uncertainties in these machine components are of particular interest, as:

- DTRT extends VMAT by the combination of dynamic rotations in these machine components.
- The beam direction is defined by both gantry and table angles, and the effect of uncertainties in these components are difficult to predict due to their dynamic movement.
- The complexity of DTRT treatment plans obstructs how the combination of uncertainties in the dynamic movement of gantry, table and collimator affects the dosimetric plan quality.

In this work, a plan is defined to be dosimetrically robust when $D98\%_{CTV}$ of the clinical target volume (CTV) is not decreased and $D2\%_{CTV}$ is not increased by more than 1 Gy compared to the nominal scenario (no uncertainty). Additionally, $D2\%_{serial\ OAR}$ and $Dmean_{parallel\ OAR}$ are not increased by 1 Gy compared to the nominal scenario. The robustness tool returns a robustness summary of all uncertainty scenarios using the robustness index (RI). RI is given by the fraction of uncertainty scenarios passing the beforementioned criteria.

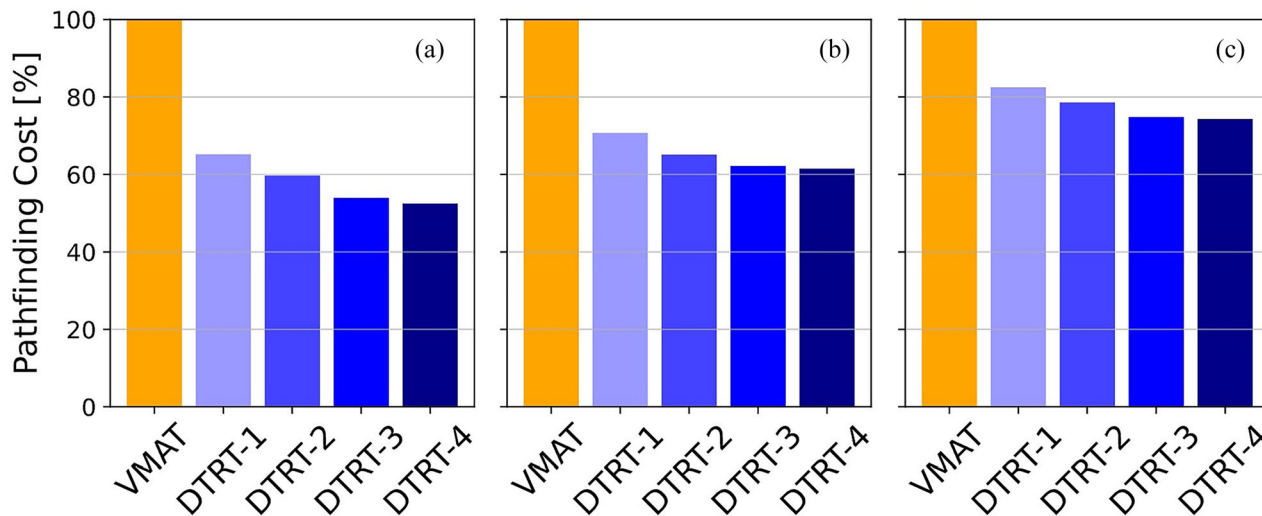


FIGURE 4 A* path finding costs on the target-OAR overlap maps for the investigated cases A, B and C, normalized to the VMAT plan as reference. The VMAT cost is calculated on each of the respective target-OAR overlap maps and summed together.

2.3.4 | Deliverability and delivery accuracy

To demonstrate the deliverability of DTRT plans of different G_{max} & ΔG_{max} , all plans are translated into XML-files and delivered in Developer Mode on a TrueBeam (Varian Medical Systems, Palo Alto, CA, USA).

It is first assessed whether the plans can be delivered collision and interlock free. Second, a machine logfile analysis is then conducted to assess the accuracy of the delivery with respect to G_{max} & ΔG_{max} . In the logfile, the *expected* and *actual* machine positions of gantry angle, table rotation angle, collimator angle and MLC are recorded at a rate of 50 Hz. The differences between expected and actual are compared, and correlations between the differences and the respective machine component speed are investigated. Third, the accuracy of the dose calculation for the extended TPP is verified by means of an end-to-end test using film validation measurements for all DTRT plans of case A (Supplementary Material 3).

2.3.5 | Delivery time

The delivery time of a plan is extracted from the machine logfiles, defined as the total beam-on time.

3 | RESULTS

3.1 | Path generation and complexity

In Figure 4 the path costs of the target-OAR overlap maps of the different plans are displayed. With increasing G_{max} and ΔG_{max} a greater reduction of the cost is achieved as expected.

In Figure 5, the paths of the three dynamic trajectories of DTRT-1, 2, 3, and 4 are shown for case A. Increasing G_{max} enabled the A* algorithm to find paths with greater GT rotation gradients: For instance, shortly after gantry angle = 0°, path 1 and path 3 of DTRT-3 and DTRT-4 include a greater table rotation range to avoid a high-cost region. By increasing ΔG_{max} , the A* algorithm is free to select a more “unsmooth” path, which is particularly seen around table = 60° and gantry = -90° of the GT map of paths 1 and 2. Furthermore, several direction changes occur at the end of the path.

Regarding complexity (Supplementary Material 4), the average and maximal G & ΔG increased from DTRT-1 to DTRT-4 plans. The average G & ΔG are 0.421 & 0.002, 0.778 & 0.003, 1.284 & 0.003 and 1.953 & 0.009 and the maximal G & ΔG are 0.580 & 0.049, 1.083 & 0.077, 3.048 & 0.178 and 3.077 & 0.499 for DTRT-1 to DTRT-4, respectively. The logfile reported maximal G and ΔG values are slightly greater than specified in the path finding, which is explained by rounding uncertainties and the internal machine translation of the XML plan-file into the application of the plan. The median MCS decreases from VMAT to the DTRT plans (0.24 to 0.19 ± 0.15).

3.2 | Dosimetric plan quality and robustness

To analyze the dosimetric plan quality, first the DVHs are compared. In Figure 6 DVHs of the plans for case A are shown. The greater freedom in the GT rotation gradient is reflected in the DVH: while PTV coverage and homogeneity is similar between all plans, OAR sparing, particularly sparing of the optic chiasm and the right optic nerve are improved substantially with

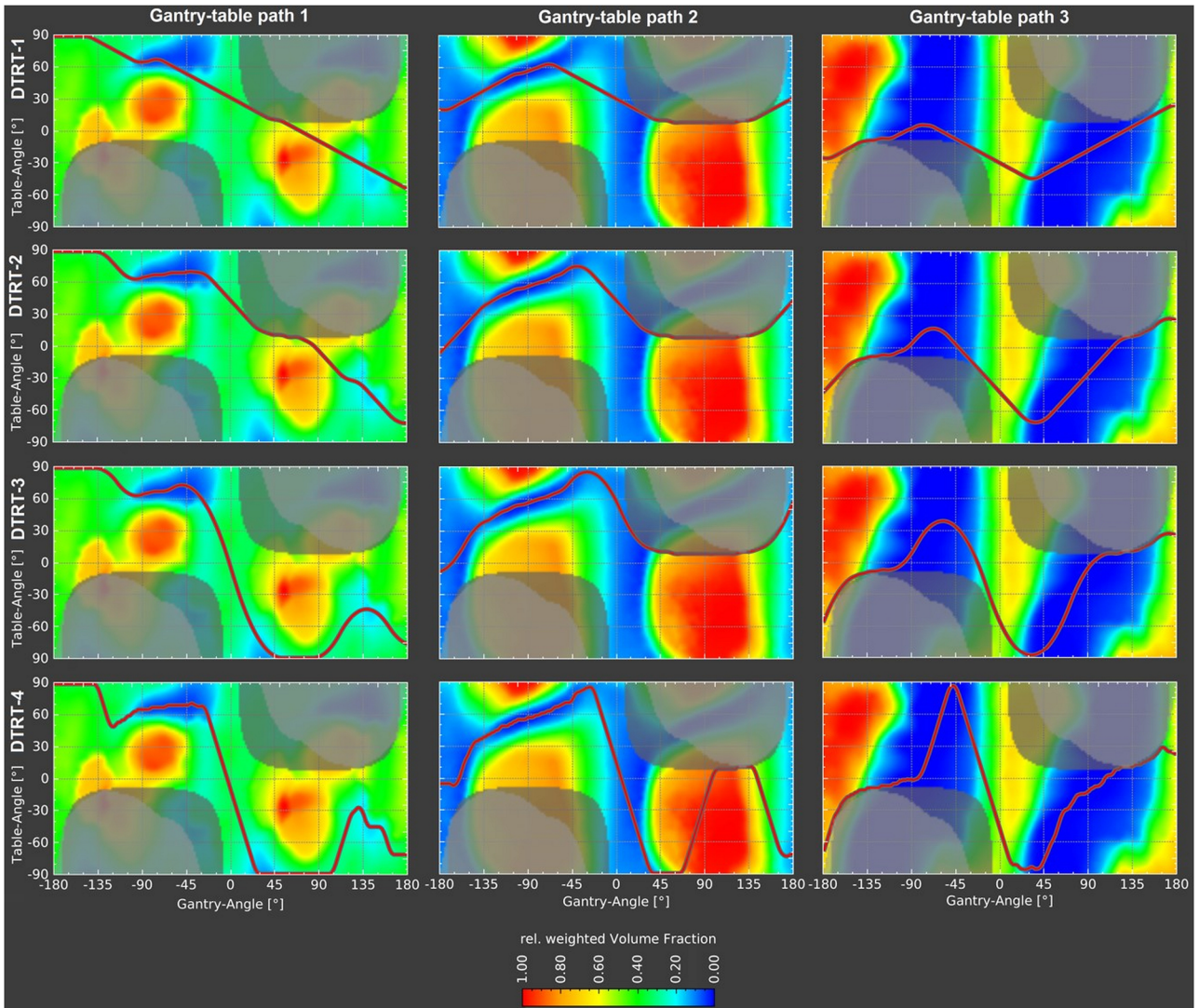


FIGURE 5 Target-OAR overlap maps with respective DTRT-1 to DTRT-4 paths for case A. With increasing freedom in the GT rotation gradient, the cost for one path is minimized more. In light grey collision zones (between gantry-patient or GT) and in dark grey CT restriction zones are marked.

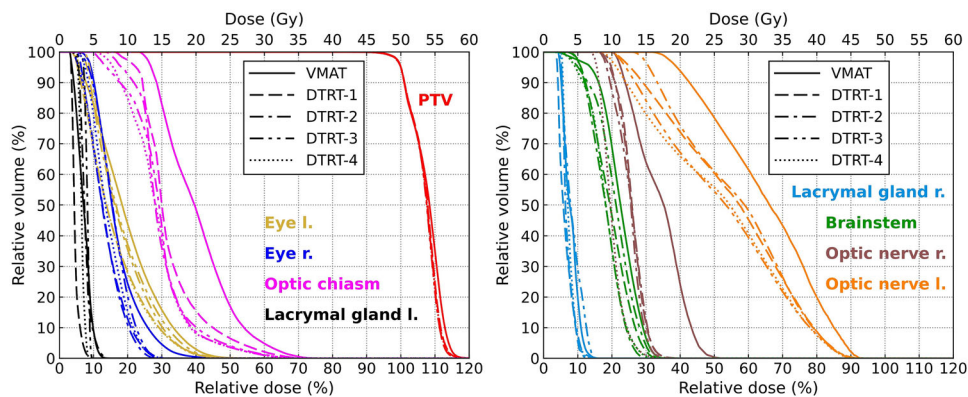


FIGURE 6 DVH comparison of the VMAT and DTRT plans for case A. While target coverage is comparable, increased OAR sparing for the OARs considered in the target overlap maps is observed with increased GT rotation gradient.

TABLE 3 Low dose bath V_5 $G_{y,NT}$ and V_{10} $G_{y,NT}$, and conformity (PI and $PI_{50\%}$) comparison of the different treatment plans of case A, B, and C. The best values (smallest volume or greatest PI and $PI_{50\%}$) are marked in bold.

	VMAT	DTRT-1	DTRT-2	DTRT-3	DTRT-4
Case A					
(V_{PTV} 63.7 cm³)					
V_{10} $G_{y,NT}$ [cm ³]	801.1	639.7	608.8	574.8	619.5
V_5 $G_{y,NT}$ [cm ³]	1469.2	1539.2	1492.4	1423.7	1477.9
PI	0.83	0.79	0.81	0.81	0.81
$PI_{50\%}$	0.25	0.30	0.31	0.31	0.31
Case B					
(V_{PTV} 272.4 cm³)					
V_{10} $G_{y,NT}$ [cm ³]	1520.4	1325.9	1260.8	1341.1	1371.3
V_5 $G_{y,NT}$ [cm ³]	1887.2	2057.4	2154.5	2325.6	2402.2
PI	0.48	0.49	0.49	0.49	0.49
$PI_{50\%}$	0.41	0.48	0.48	0.49	0.49
Case C					
(V_{PTV} 410.8 cm³)					
V_{10} $G_{y,NT}$ [cm ³]	2188.5	2409.7	3074.1	3248.6	3282.3
V_5 $G_{y,NT}$ [cm ³]	2897.8	4583.0	5310.6	5459.4	5383.2
PI	0.84	0.84	0.83	0.84	0.84
$PI_{50\%}$	0.29	0.31	0.31	0.31	0.31

increasing G_{max} & ΔG_{max} ($D_{0.03cm^3, optic\ nerve\ r.}$ -9.3 Gy). The DTRT-2 plan for case B improves the OAR sparing the best: $D_{0.03cm^3, optic\ nerve\ r.}$ -1.6 Gy, $D_{0.03cm^3, eye\ l.}$ -6.0 Gy, $D_{0.03cm^3, chiasm}$ -7.7 Gy, $D_{mean, brain}$ -4.7 Gy compared to VMAT (Supplementary Material 5). Only slight improvements with increasing G_{max} & ΔG_{max} are observed for the plans of case C ($D_{mean, parotid\ l.}$ -1.0 Gy) at the cost of increased mean dose (>5 Gy) to the brain (Supplementary Material 6).

The low dose bath in terms of V_{10} $G_{y,NT}$ is reduced for case A and case B from VMAT to DTRT, but increases for case C. Except for case A, V_5 $G_{y,NT}$ is increased with increasing G_{max} & ΔG_{max} . The conformity of the prescribed isodose line differs by maximum of 0.01, except for case A, where it decreases by 0.04 from VMAT to DTRT-1. Improved conformity for the 50% isodose line is observed for the DTRT plans (Table 3).

The dosimetric robustness (Figure 7) to patient setup uncertainties is similar between all plans for all cases. Furthermore, there is no clear trend of dosimetric robustness with respect to the GT rotation gradient. The DTRT plans of case A and B are more robust to machine uncertainties than the VMAT plans. For case C, dosimetric robustness to the investigated machine uncertainties decreases with increasing freedom in the GT rotation gradient.

When considering only the CTV robustness criteria (RI_{CTV}), the RI_{CTV} for systematic (random) setup uncertainties for case A, B, and C are $>25\%$ (100%), 100% (100%), and $>40\%$ (100%), respectively. The robustness of the CTV for the VMAT plan of case C to systematic

setup uncertainties is substantially worse (40%) as compared to the DTRT plans ($>88\%$). Regarding machine uncertainties up to $\pm 4^\circ$, the CTV robustness of the plans for case A is little influenced and have an $RI_{CTV} > 95\%$. The larger targets of case B and C have an RI_{CTV} of $>71\%$ and $>24\%$. For uncertainties up to $\pm 1^\circ$ RI_{CTV} is 100% for all plans and cases.

3.3 | Deliverability

3.3.1 | Logfile analysis & film measurements

The distributions of table rotation, gantry rotation and MLC position uncertainties retrieved from the recorded logfiles are shown in Figure 8. The observed increase of the average G and ΔG from DTRT-1 to DTRT-4 has no substantial effect on the uncertainty distribution of the gantry, table and collimator rotation. The average root-mean-square (RMS) uncertainty of the moving MLC leaves decreases with increasing G_{max} & ΔG_{max} . A correlation analysis of machine component speed and uncertainty in the respective machine component is found in the Supplementary Material 7.

The film measurements for the DTRT plans of case A agree with the respective dose calculations by $>96\%$ Gamma passing rate (Supplementary Material 3). No substantial differences between the measurements of the DTRT-1 to DTRT-4 plans are observed.

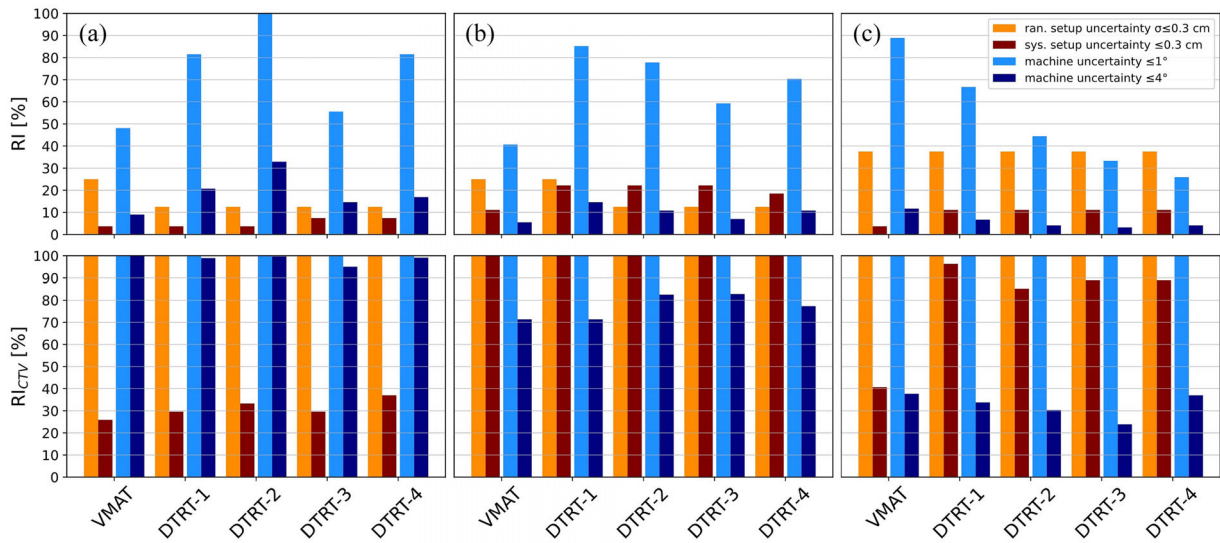


FIGURE 7 Dosimetric robustness, expressed in terms of RI and RI_{CTV} to random and systematic patient setup uncertainties in lateral, longitudinal, and vertical direction up to ± 0.3 cm, as well as systematic uncertainties in gantry, table and collimator rotation between $\pm 1^\circ$ and $\pm 4^\circ$ for the plans of case A (a, left), case B (b, middle) and case C (c, right).

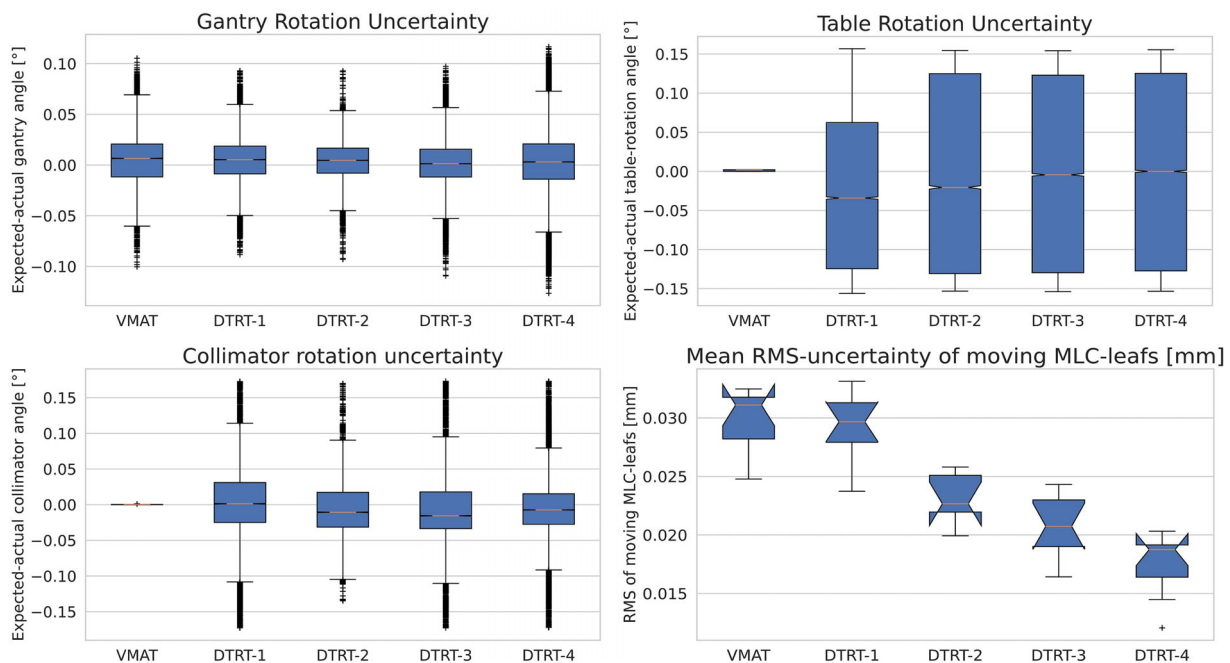


FIGURE 8 TrueBeam machine logfile analysis for the VMAT and DTRT plans. Small offsets for table and collimator rotation, observed in the VMAT plans, are not corrected, as they are within the precision limit of the respective machine component.

3.3.2 | Delivery time

With increasing G_{max} and ΔG_{max} , the mean time to deliver one arc/dynamic trajectory increases by a factor of 2 from 1.05 to 2.1 min (Figure 9). Of note is that VMAT and DTRT-1 have similar delivery times. In our institution, the TrueBeam has a maximal gantry rotation and table rotation speed of 6 °/s and 3 °/s, respectively, leading to

a G_{max} of 0.5 (as in DTRT-1), so that the table rotation does not slow down the delivery.

4 | DISCUSSION

The impact of the GT rotation gradient on plan quality was comprehensively assessed by evaluation of

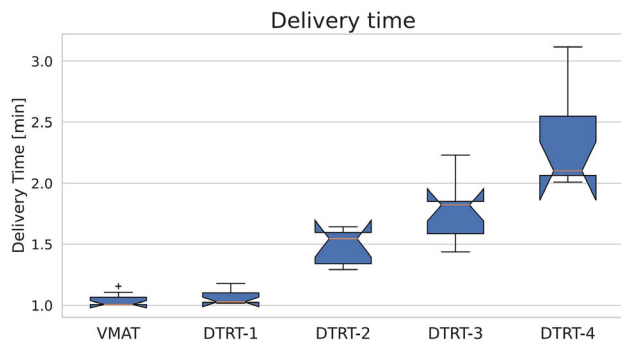


FIGURE 9 Delivery time per arc and dynamic trajectory of the VMAT and DTRT-1 to DTRT-4 plans.

dosimetric plan quality, complexity, dosimetric robustness, deliverability, and delivery time for three cases in the head and neck, and brain region.

4.1 | Path generation and complexity

With the extended DTRT TPP, the dynamics of DTRT can be characterized and the user has more control of DTRT path generation. This developed approach has three main benefits: *First*, it provides a fast and optimal path finding solution on a given cost map. For the presented cases, path finding took less than 4 min to provide the path with the minimal cost.³⁴ *Second*, G_{max} and ΔG_{max} enable user control over the dynamics of the determined paths, tailoring DTRT plans to machine and institution specific requirements. G_{max} controls delivery slow-down due to the finite table rotation speed. ΔG_{max} regulates the smoothness of the path and enables to avoid multiple disruptive directional changes in table rotation. It is expected that a smoother path has a beneficial effect on the lifespan of the machine components. *Third*, the developed approach is applicable to a variety of path finding strategies and is not limited to a specific type of cost map (e.g., target-OAR overlap as presented in this work). The cost map is interchangeable and could for instance also comprise dosimetric information for dosimetric guided path finding.³⁵ However, approaches that include dosimetric information³⁶ need considerably more computation time. The path finding would also include the computationally expensive dose calculation or even intensity optimization.

G and ΔG complement the frequently used MCS, which has been related to delivery accuracy,^{28,37} in characterizing the dynamics and complexity of DTRT plans. While MCS decreases slightly from VMAT to DTRT-1 for the investigated cases, it does not decrease further with increasing G_{max} & ΔG_{max} .

4.2 | Dosimetric plan quality and robustness

The applied TPP in this work is sequential: first, target-OAR overlap maps generation and path finding, and second, the intensity optimization along the DTRT path. Due to this sequential nature, the dosimetric plan quality does not necessarily correlate with the decrease in path finding cost. Other approaches employ simultaneous optimization of path and intensity modulation at the cost of increased optimization times.^{38–40} However, regarding dosimetric plan quality, this work agrees with previous findings.^{19,41,42} The generated DTRT plans of this work have the potential to substantially spare OARs as compared to the VMAT reference plans, particularly the ones considered in the target-OAR overlap maps. Increasing G_{max} & ΔG_{max} , enables improved sparing for these OARs, especially for case A and B. For case C, the DTRT plans also reduce dose to OARs considered in the target-OAR overlap, but at the cost of increased mean dose to the brain due to the large size and location of the target (lower head and neck area). Little variation in the dose conformity to the target is observed,⁴¹ with PI differing at most by 0.01, except for case A where the PI decreased by 0.04 from VMAT to DTRT-1. However, $PI_{50\%}$ is reduced for all cases from VMAT to DTRT. Furthermore, concerns regarding an increased low dose bath for non-coplanar delivery techniques⁸ might not be justified, as for the DTRT plans a reduction up to 3% of $V_{5\text{ Gy,NT, case A}}$, 28% of $V_{10\text{ Gy,NT, case A}}$, and 17% of $V_{10\text{ Gy,NT, case B}}$ is achieved compared to the respective VMAT plans.

Previous robustness considerations for non-coplanar photon-based treatment techniques are limited and have primarily focused on patient-setup uncertainties^{8,22,23} and on the evaluation of the target dose. In these previous studies, it is indicated that non-coplanar techniques, are equally or more robust than coplanar VMAT. This work agrees by confirming that, except for case C, there is no substantial difference in the dosimetric target robustness for the investigated plans and setup uncertainties, regardless their GT rotation gradient. This work further extends these investigations by evaluating the robustness of OAR sparing and the impact of uncertainties in gantry, table and collimator, on the planned dose distribution. The investigated machine uncertainties are several magnitudes larger than the uncertainties reported in the machine logfiles. However, systematic miscalibration of the treatment machines are not reported in the machine logfiles. Miscalibrations might be only detectable during machine QA. Furthermore, they are chosen for exploratory purposes to simulate scenarios that surpass the published machine tolerance limits.⁴³ On a different note, concerns about the robustness to rotational setup

uncertainties are addressed by interpreting the table rotation uncertainty as patient-setup uncertainty. Plans of case A and B with increased G_{max} & ΔG_{max} show improved robustness to machine uncertainties, which is linked to their lower low dose bath. The impact of the uncertainties on the dose distribution happens on a smaller dose scale. The results of case C confirm this explanation, as the VMAT plan has the smallest low dose bath and the highest RI. The CTV robustness is hardly sensitive to random patient-setup uncertainties up to 0.3 cm and to machine uncertainties up to 1°. The PTV margin prevents a deterioration of the CTV dose in most cases. Of note is that in a clinical DTRT delivery setting, patient and machine uncertainties would occur together and a robustness evaluation would need to consider both uncertainty types in combination. Furthermore, uncertainties in patient setup might be influenced by the GT rotation gradient.

4.3 | Deliverability and delivery time

This work focuses on plan deliverability, and all created plans have been delivered interlock-free. Additionally, film measurements confirm the accuracy of the dose calculation algorithm²⁶ for the extended TPP and verify the accurate delivery of the plans of different GT rotation gradient on the TrueBeam by means of an end-to-end test. Analysis of the machine logfiles confirmed the results of previous assessments.^{42,44} Uncertainties in MLC leaf position are correlated to the leaf speed. Additionally, strong correlations are observed between table/collimator rotation uncertainty and rotation speed. However, an increase in G_{max} & ΔG_{max} is not accompanied by greater mean uncertainties in the respective machine components for the investigated plans. The average RMS error for the moving MLC leaves even decreases with increasing G_{max} & ΔG_{max} and lower MCS. One possible explanation is that the MLC leaves have more time to achieve the desired apertures when there is more table rotation, as the table rotation speed with 3°/s can slow the treatment delivery down.

The delivery time increases with increasing GT rotation gradient for the investigated cases. However, by setting G_{max} to 0.5, the additional dynamic table rotation does not slow the delivery down, while the plan quality still profits from the dosimetric benefits of the non-coplanar beam directions. In the context of overall treatment time, which includes the setup and positioning of the patient, also the delivery times of the DTRT-2 trajectories are comparably small.^{45,46}

5 | CONCLUSION

This work presents a method to generate DTRT plans with user-defined GT rotation gradients. The impact of

this gradient on plan quality is comprehensively analyzed and the trade-offs between dosimetric plan quality, complexity, deliverability, delivery time and dosimetric robustness are highlighted. A small increase in this gradient, from VMAT to DTRT-1 ($G_{max} = 0.5$), can already improve OAR sparing due to the non-coplanar beam directions. Furthermore, smooth delivery (by $\Delta G_{max} = 0.125$) and similar delivery times as VMAT are maintained. Increasing the gradient and its change further shows no substantial improvements in dosimetric plan quality. Considering that the GT rotation gradient can impact patient comfort and machine durability, it is critical to have the option to limit G and ΔG for clinical acceptable delivery times and smooth delivery. Finally, this research confirms the feasibility of planning, accurately calculating, and delivering DTRT plans of different GT rotation gradients.

ACKNOWLEDGEMENTS


This work was supported by Varian, a Siemens Healthineers Company. The MC dose calculations were performed on UBELIX (www.id.unibe.ch/hpc), the high-performance-computing cluster at the University of Bern.

Open access funding provided by Inselspital Universitätsspital Bern.

CONFLICT OF INTEREST STATEMENT

The authors have no relevant conflicts of interest to disclose. In his role as deputy editor for Medical Physics, author M.K.F. was blinded to the review process and had no role in decisions pertaining to this manuscript.

ORCID

Hannes A. Loebner 

<https://orcid.org/0000-0002-8439-2464>

Silvan Mueller 

<https://orcid.org/0000-0002-9835-4362>

Philipp Wallimann 

<https://orcid.org/0000-0002-7110-6617>

Daniel M. Aebbersold 

<https://orcid.org/0000-0002-9493-3834>

Marco F. M. Stampanoni 

<https://orcid.org/0000-0001-7486-6681>

Michael K. Fix 

<https://orcid.org/0000-0002-3911-3403>

Peter Manser 

<https://orcid.org/0000-0003-3225-8025>

REFERENCES

1. Otto K. Volumetric modulated arc therapy: IMRT in a single gantry arc. *Med Phys*. 2008;35(1):310-317. doi:10.1118/1.2818738
2. Verbakel WFAR, Cuijpers JP, Hoffmans D, Bieker M, Slotman BJ, Senan S. Volumetric intensity-modulated arc therapy vs. conventional IMRT in head-and-neck cancer: a comparative

- planning and dosimetric study. *Int J Radiat Oncol Biol Phys*. 2009;74(1):252-259. doi:10.1016/j.ijrobp.2008.12.033
3. Teoh M, Clark CH, Wood K, Whitaker S, Nisbet A. Volumetric modulated arc therapy: a review of current literature and clinical use in practice. *Br J Radiol*. 2011;84(1007). doi:10.1259/bjr/22373346
 4. Smyth G, Evans PM, Bamber JC, et al. Non-coplanar trajectories to improve organ at risk sparing in volumetric modulated arc therapy for primary brain tumors. *Radiother Oncol*. 2016;121(1):124-131. doi:10.1016/j.radonc.2016.07.014
 5. Park J, Park JW, Yea JW. Non-coplanar whole brain radiotherapy is an effective modality for parotid sparing. *Yeungnam Univ J Med*. 2019;36(1):36. doi:10.12701/YUJM.2019.00087
 6. Fogliata A, Clivio A, Nicolini G, Vanetti E, Cozzi L. A treatment planning study using non-coplanar static fields and coplanar arcs for whole breast radiotherapy of patients with concave geometry. *Radiother Oncol*. 2007;85(3):346-354. doi:10.1016/j.radonc.2007.10.006
 7. Sheng K, Shepard DM. Point/Counterpoint. Noncoplanar beams improve dosimetry quality for extracranial intensity modulated radiotherapy and should be used more extensively. *Med Phys*. 2015;42(2):531-533. doi:10.1118/1.4895981
 8. Gayen S, Kombathula SH, Manna S, Varshney S, Pareek P. Dosimetric comparison of coplanar and non-coplanar volumetric-modulated arc therapy in head and neck cancer treated with radiotherapy. *Radiat Oncol J*. 2020;38(2):138. doi:10.3857/ROJ.2020.00143
 9. Ohira S, Ueda Y, Akino Y, et al. HyperArc VMAT planning for single and multiple brain metastases stereotactic radiosurgery: a new treatment planning approach. *Radiat Oncol*. 2018;13(1):1-9. doi:10.1186/S13014-017-0948-Z
 10. Kadoya N, Abe Y, Kajikawa T, et al. Automated noncoplanar treatment planning strategy in stereotactic radiosurgery of multiple cranial metastases: hyperArc and CyberKnife dose distributions. *Med Dosimetry*. 2019;44(4):394-400. doi:10.1016/J.MEDDOS.2019.02.004
 11. Tran A, Zhang J, Woods K, et al. Treatment planning comparison of IMPT, VMAT and 4π radiotherapy for prostate cases. *Radiat Oncol*. 2017;12(1):1-9. doi:10.1186/S13014-016-0761-0
 12. Rwigema JCM, Nguyen D, Heron DE, et al. 4π noncoplanar stereotactic body radiation therapy for head-and-neck cancer: potential to improve tumor control and late toxicity. *Int J Radiat Oncol Biol Phys*. 2015;91(2):401-409. doi:10.1016/J.IJROBP.2014.09.043
 13. Dong P, Lee P, Ruan D, et al. 4π non-coplanar liver SBRT: a novel delivery technique. *Int J Radiat Oncol Biol Phys*. 2013;85(5):1360-1366. doi:10.1016/J.IJROBP.2012.09.028
 14. Murzin VL, Woods K, Moiseenko V, et al. 4π plan optimization for cortical-sparing brain radiotherapy. *Radiother Oncol*. 2018;127(1):128-135. doi:10.1016/J.RADONC.2018.02.011
 15. Woods K, Nguyen D, Tran A, et al. Viability of noncoplanar VMAT for liver SBRT compared with coplanar VMAT and beam orientation optimized 4π IMRT. *Adv Radiat Oncol*. 2016;1(1):67-75. doi:10.1016/J.ADRO.2015.12.004
 16. Yu VY, Landers A, Woods K, et al. A prospective 4π radiation therapy clinical study in recurrent high-grade glioma patients. *Int J Radiat Oncol Biol Phys*. 2018;101(1):144-151. doi:10.1016/J.IJROBP.2018.01.048
 17. Papp D, Bortfeld T, Unkelbach J. A modular approach to intensity-modulated arc therapy optimization with noncoplanar trajectories. *Phys Med Biol*. 2015;60(13):5179-5198. doi:10.1088/0031-9155/60/13/5179
 18. Smyth G, Evans PM, Bamber JC, Bedford JL. Recent developments in non-coplanar radiotherapy. *Br J Radiol*. 2019;92(1097). doi:10.1259/BJR.20180908
 19. Fix MK, Frei D, Volken W, et al. Part 1: optimization and evaluation of dynamic trajectory radiotherapy. *Med Phys*. 2018;45(9):4201-4212. doi:10.1002/mp.13086
 20. Manser P, Frauchiger D, Frei D, Volken W, Terrilini D, Fix MK. Dose calculation of dynamic trajectory radiotherapy using Monte Carlo. *Z Med Phys*. 2019;29(1). doi:10.1016/j.zemedi.2018.03.002
 21. Hernandez V, Hansen CR, Widesott L, et al. What is plan quality in radiotherapy? The importance of evaluating dose metrics, complexity, and robustness of treatment plans. *Radiother Oncol*. 2020;153:26-33. doi:10.1016/j.radonc.2020.09.038
 22. Sagawa T, Ohira S, Ueda Y, et al. Dosimetric effect of rotational setup errors in stereotactic radiosurgery with HyperArc for single and multiple brain metastases. *J Appl Clin Med Phys*. 2019;20(10):84-91. doi:10.1002/ACM2.12716
 23. Calmels L, Blak Nyrup Biancardo S, Sibolt P, et al. Single-isocenter stereotactic non-coplanar arc treatment of 200 patients with brain metastases: multileaf collimator size and setup uncertainties. *Strahlenther Onkol*. 2022;198(5):436-447. doi:10.1007/s00066-021-01846-6
 24. González Á. Measurement of areas on a sphere using fibonacci and latitude-longitude lattices. *Math Geosci*. 2009;42(1):49-64. doi:10.1007/S11004-009-9257-X
 25. Hart PE, Nilsson NJ, Raphael B. A formal basis for the heuristic determination of minimum cost paths. *IEEE Trans Syst Sci Cyber*. 1968;4(2):100-107. doi:10.1109/TSSC.1968.300136
 26. Fix MK, Manser P, Frei D, Volken W, Mini R, Born EJ. An efficient framework for photon Monte Carlo treatment planning*. *Phys Med Biol*. 2007;52(19):N425. doi:10.1088/0031-9155/52/19/N01
 27. Kawrakow I, Fippel M. VMC, a fast MC algorithm for radiation treatment planning. *Use Comp Radiat Ther*. doi:10.1007/978-3-642-59758-9_46. Published online 2000:126-128.
 28. McNiven AL, Sharpe MB, Purdie TG. A new metric for assessing IMRT modulation complexity and plan deliverability. *Med Phys*. 2010;37(2):505-515. doi:10.1118/1.3276775
 29. Masi L, Doro R, Favuzza V, Cipressi S, Livi L. Impact of plan parameters on the dosimetric accuracy of volumetric modulated arc therapy. *Med Phys*. 2013;40(7):071718. doi:10.1118/1.4810969
 30. Paddick I. A simple scoring ratio to index the conformity of radiosurgical treatment plans. Technical note. *J Neurosurg*. 2000;93:219-222. doi:10.3171/JNS.2000.93.SUPPLEMENT
 31. Loebner HA, Volken W, Mueller S, et al. Development of a Monte Carlo based robustness calculation and evaluation tool. *Med Phys*. doi:10.1002/MP.15683. Published online May 4, 2022.
 32. Kanakavelu N, Samuel JJ. Determination of patient set-up error and optimal treatment margin for intensity modulated radiotherapy using image guidance system. *JBUON*. 2016;2(21).
 33. Delishaj D, Ursino S, Pasqualetti F, et al. Set-up errors in head and neck cancer treated with IMRT technique assessed by cone-beam computed tomography: a feasible protocol. *Radiat Oncol J*. 2018;36(1):54. doi:10.3857/ROJ.2017.00493
 34. Mathew GE. Direction based heuristic for pathfinding in video games. *Procedia Comput Sci*. 2015;47(C):262-271. doi:10.1016/J.PROCS.2015.03.206
 35. Mackeprang P, Bertholet J, Mueller S, et al. MO-0544 4pi-IMRT based path-finding for dynamic trajectory radiotherapy. *Radiother Oncol*. 2022;170:S469-S470. doi:10.1016/S0167-8140(22)02378-7
 36. Rocha H, Dias J, Ventura T, Ferreira B, do Carmo, Lopes M. An optimization approach for noncoplanar intensity-modulated arc therapy trajectories. *Lecture Notes in Computer Science (including subseries Lecture Notes in Artificial Intelligence and Lecture Notes in Bioinformatics)*. 2019:199-214. doi:10.1007/978-3-030-24302-9_15. 11621 LNCS
 37. Jubbier ON, Abdullah SS, Alabedi HH, Alazawy NM, MJ Al-Musawi. The effect of modulation complexity score (MCS) on the IMRT treatment planning delivery accuracy. *J Phys Conf Ser*. 2021;1829(1):012017. doi:10.1088/1742-6596/1829/1/012017

38. Meedt G, Alber M, Nüsslin F. Non-coplanar beam direction optimization for intensity-modulated radiotherapy. *Phys Med Biol.* 2003;48(18):2999. doi:10.1088/0031-9155/48/18/304
39. Dong P, Liu H, Xing L. Monte Carlo tree search -based non-coplanar trajectory design for station parameter optimized radiation therapy (SPORT). *Phys Med Biol.* 2018;63(13):135014. doi:10.1088/1361-6560/AACA17
40. Mullins J, Renaud MA, Serban M, Seuntjens J. Simultaneous trajectory generation and volumetric modulated arc therapy optimization. *Med Phys.* 2020;47(7):3078-3090. doi:10.1002/MP.14155
41. Bertholet J, Mackeprang PH, Mueller S, et al. Organ-at-risk sparing with dynamic trajectory radiotherapy for head and neck cancer: comparison with volumetric arc therapy on a publicly available library of cases. *Radiat Oncol.* 2022;17(1):122. doi:10.1186/S13014-022-02092-5
42. Loebner HA, Frauchiger D, Mueller S, et al. Technical note: feasibility of gating for dynamic trajectory radiotherapy – Mechanical accuracy and dosimetric performance. *Med Phys.* 2023. doi:10.1002/mp.16533
43. Barnes MP, Greer PB. Evaluation of the truebeam machine performance check (MPC): mechanical and collimation checks. *J Appl Clin Med Phys.* 2017;18(3):56-66. doi:10.1002/ACM2.12072
44. Olasolo-Alonso J, Vázquez-Galiñanes A, Pellejero-Pellejero S, Pérez-Azorín JF. Evaluation of MLC performance in VMAT and dynamic IMRT by log file analysis. *Phys Med.* 2017;33:87-94. doi:10.1016/J.EJMP.2016.12.013
45. Studenski MT, Bar-Ad V, Siglin J, et al. Clinical experience transitioning from IMRT to VMAT for head and neck cancer. *Med Dosimetry.* 2013;38(2):171-175. doi:10.1016/J.MEDDOS.2012.10.009
46. Ballangrud Å, Kuo LC, Happersett L, et al. Institutional experience with SRS VMAT planning for multiple cranial metastases. *J Appl Clin Med Phys.* 2018;19(2):176-183. doi:10.1002/ACM2.12284

SUPPORTING INFORMATION

Additional supporting information can be found online in the Supporting Information section at the end of this article.

How to cite this article: Loebner HA, Mueller S, Volken W, et al. Impact of the gradient in gantry-table rotation on dynamic trajectory radiotherapy plan quality. *Med Phys.* 2023;1-14. <https://doi.org/10.1002/mp.16749>